Check for updates

Received: 1 March 2023 | Revised: 30 June 2023 | Accepted: 11 July 2023

DOI: 10.1111/nan.12925

ORIGINAL ARTICLE

Neuropathology and Applied Neurobiology
JOURNAL OF THE BRITISH NEUROPATHOLOGICAL SOCIETY

WILEY

Neuromuscular junction denervation and terminal Schwann cell loss in the hTDP-43 overexpression mouse model of amyotrophic lateral sclerosis

Abrar Alhindi[1,2,3] | Megan Shand[1,2] | Hannah L. Smith[1,2] | Ana S. Leite[1,2,4] | Yu-Ting Huang[1,2] | Dinja van der Hoorn[1,2] | Zara Ridgway[1,2] | Kiterie M. E. Faller[1,2,5] | Ross A. Jones[1,2] | Thomas H. Gillingwater[1,2] | Helena Chaytow[1,2]

[1]Edinburgh Medical School: Biomedical Sciences, University of Edinburgh, Edinburgh, UK

[2]Euan MacDonald Centre for Motor Neuron Disease Research, Edinburgh, UK

[3]Faculty of Medicine, Department of Anatomy, King Abdulaziz University, Jeddah, Saudi Arabia

[4]School of Medicine, UNESP-São Paulo State University, Botucatu, Sao Paulo, Brazil

[5]Royal (Dick) School of Veterinary Studies, University of Edinburgh, Edinburgh, UK

Correspondence
Helena Chaytow, Euan MacDonald Centre for Motor Neuron Disease Research, Edinburgh, UK.
Email: helena.chaytow@ed.ac.uk

Funding information
King Abdulaziz University; MND Scotland; My Name'5 Doddie Foundation

Abstract

Aims: Amyotrophic lateral sclerosis (ALS) is a fatal neurodegenerative disease with complex aetiology. Despite evidence of neuromuscular junction (NMJ) denervation and 'dying-back' pathology in models of SOD1-dependent ALS, evidence in other genetic forms of ALS is limited by a lack of suitable animal models. TDP-43, a key mediator protein in ALS, is overexpressed in neurons in Thy1-hTDP-43^{WT} mice. We therefore aimed to comprehensively analyse NMJ pathology in this model of ALS.

Methods: Expression of TDP-43 was assessed via western blotting. Immunohistochemistry techniques, alongside NMJ-morph quantification, were used to analyse motor neuron number, NMJ denervation status and terminal Schwann cell morphology.

Results: We present a time course of progressive, region-specific motor neuron pathology in Thy1-hTDP-43^{WT} mice. Thy1-driven hTDP-43 expression increased steadily, correlating with developing hindlimb motor weakness and associated motor neuron loss in the spinal cord with a median survival of 21 days. Pronounced NMJ denervation was observed in hindlimb muscles, mild denervation in cranial muscles but no evidence of denervation in either forelimb or trunk muscles. NMJ pathology was restricted to motor nerve terminals, with denervation following the same time course as motor neuron loss. Terminal Schwann cells were lost from NMJs in hindlimb muscles, directly correlating with denervation status.

Conclusions: Thy1-hTDP-43^{WT} mice represent a severe model of ALS, with NMJ pathology/denervation of distal muscles and motor neuron loss, as observed in ALS patients. This model therefore provides an ideal platform to investigate mechanisms of dying-back pathology, as well as NMJ-targeting disease-modifying therapies in ALS.

KEYWORDS
amyotrophic lateral sclerosis, motor neuron disease, NMJ denervation, TDP-43 proteinopathies, transgenic mouse

Abrar Alhindi, Megan Shand and Hannah L. Smith contributed equally to this work as first authors. Thomas H. Gillingwater and Helena Chaytow contributed equally to this work as last authors.

This is an open access article under the terms of the Creative Commons Attribution License, which permits use, distribution and reproduction in any medium, provided the original work is properly cited.
© 2023 The Authors. *Neuropathology and Applied Neurobiology* published by John Wiley & Sons Ltd on behalf of British Neuropathological Society.

INTRODUCTION

Amyotrophic lateral sclerosis (ALS) is a fatal neurodegenerative disease characterised by loss of both upper and lower motor neurons. This loss of motor neurons leads to progressive paralysis, muscle weakness and atrophy, with premature death usually resulting from respiratory failure [1]. ALS has both familial and sporadic aetiology, with familial cases accounting for around 10% of patients. Several mutations have been linked to familial ALS, in genes such as *SOD1*, *C9ORF72*, *FUS* and *TARDBP*, whereas the majority of sporadic ALS cases have no clear genetic cause [2].

Lower motor neurons are highly specialised cells, with long axons running between the cell body in the ventral horn of the spinal cord and the neuromuscular junction (NMJ) with its target skeletal muscle, making them uniquely vulnerable to damage and degeneration. Molecular pathology reported to contribute to motor neuron degeneration includes axonal dysfunction [3], defects in RNA processing and transport [4] and accumulation of toxic protein aggregates [5]. In addition to these pathways, one vital anatomical feature of the motor neuron that has been strongly implicated in ALS pathology is the NMJ, resulting in the characterisation of ALS as a 'dying-back' pathology where dysfunction at the NMJ is a primary phenotype resulting in retrograde signalling leading to the subsequent motor neuron cell death [6].

The NMJ is a highly specialised tripartite synapse comprising a presynaptic motor nerve terminal and a postsynaptic motor endplate on the muscle fibre, capped by non-myelinating terminal Schwann cells (tSCs) [7]. Structural changes at the NMJ have been reported in human ALS patients, including denervation [8] and decreased NMJ area [9], and loss of motor units represents an early event in the course of the disease [10, 11]. Because of the difficulty in acquiring human motor point biopsies, especially before the onset of symptoms, mouse models are an important experimental tool for studying this pathology. However, most studies on NMJ pathology in ALS have relied on mutant SOD1 mouse models. Although these mice do mimic ALS pathology with progressive motor dysfunction and early evidence of NMJ denervation [12], the failure of almost all drugs to translate from promising results in the SOD1 mouse into success in the clinic has led many to question the validity of the model, particularly because the mutation is only found in 1%–2% of ALS patients [2]. In the SOD1 mouse model, denervation can be seen pre-symptomatically, particularly in the *tibialis anterior* (TA) and *gastrocnemius* (GC) muscles [13], whereas denervation of the *soleus* (SOL) is not seen until later time points [14]. The SOL muscle consists mostly of 'slow' fibre types and is considered resistant in ALS pathology compared with muscles made up of fast-fatigable fibre types such as the TA, which is considered vulnerable [15]. Additionally, a recent paper has shown that fast motor neurons innervating the TA in the SOD1 mouse have selectively impaired axonal transport at early symptomatic stages, whereas slow motor neurons innervating the SOL are not affected [16]. This idea of a pattern of vulnerability based on fibre type is pervasive in ALS research, yet solely based on the SOD1 mouse. Evidence of vulnerability patterns based on models other than SOD1 are needed to confirm trends that can be applied to multiple ALS patient groups.

Key Practitioner Messages

- Thy1-hTDP-43^{WT} is a mouse model of severe ALS, with increasing expression of human TDP-43 protein leading to a progressive motor phenotype and early death
- Thy1-hTDP-43^{WT} mice develop a robust NMJ denervation phenotype, predominantly in hindlimb muscles, correlating with motor neuron loss
- Terminal Schwann cell loss correlates with NMJ denervation
- Thy1-hTDP-43^{WT} mice provide an ideal model for studying TDP-43-mediated NMJ pathology in ALS

Because of the complexity of ALS genetics, there are dozens of alternative mouse models, some of which display NMJ denervation [17]. Several models target TDP-43 (TAR DNA-binding protein 43; gene name *TARDBP*), an RNA-binding protein found to be mislocalised in pathological cytoplasmic aggregates in the neurons of >95% ALS patients [5, 18]. Importantly, these TDP-43-positive aggregates are seen in both sporadic and familial ALS patients [19], and so TDP-43 pathology represents a key feature of ALS regardless of genetic background. Mouse models overexpress either wild-type or mutant forms of TDP-43. Some models show NMJ denervation, but most studies only assess one muscle type, and denervation is often only seen at very late stages, often at time points over a year old, creating logistical difficulties [20, 21]. However, TDP-43 has been shown to contribute to axonal outgrowth and is actively transported along the axon, with some evidence of pathological localisation to the NMJ [22]. A model based on TDP-43 that shows clear NMJ pathology would therefore be valuable for future ALS research.

Given the key role of TDP-43 in ALS pathology, we have undertaken a comprehensive analysis of motor neuron and NMJ pathology in the Thy1-hTDP-43^{WT} mouse model. This mouse model recapitulates hallmarks of severe ALS with progressive paralysis and shortened lifespan, resulting from neuronal-specific overexpression of the human TDP-43 transgene under the neuronal *Thy1* promoter [23]. Motor symptoms and decreased survival in this model have already been described, along with cellular accumulation of ubiquitinated TDP-43. However, it remains unclear as to whether this mouse model represents a robust means to study TDP-43-mediated motor neuron and NMJ pathology. Additionally, the presence of motor neuron/NMJ pathology in the Thy1-hTDP-43^{WT} mouse model would allow us to establish whether the widely reported pattern of selective vulnerability in ALS, with motor neurons innervating fast-fatigable muscle types

13652990, 2023, 4, Downloaded from https://onlinelibrary.wiley.com/doi/10.1111/nan.12925 by Universidade Estadual Paulista, Wiley Online Library on [24/09/2026]. See the Terms and Conditions (https://onlinelibrary.wiley.com/terms-and-conditions) on Wiley Online Library for rules of use; OA articles are governed by the applicable Creative Commons License

being considered the most vulnerable [24], is conserved across multiple genetic forms of the disease. We have characterised motor neuron and NMJ pathology across a range of muscle groups in the Thy1-hTDP-43^{WT} mouse model, with the aim of building a regional timeline of cellular and molecular phenotypes at pre-symptomatic, early symptomatic and late symptomatic disease stages. We demonstrate changing expression levels of TDP-43 in the CNS compared with normal developmental expression and correlate this to a loss of motor neurons and selective denervation of NMJs in muscles of the hindlimb.

MATERIALS AND METHODS

Animals

Thy1-hTDP-43^{WT} overexpression mice on a mixed C57BL6/J × SJL background were purchased from Jackson labs (RRID:IMSR_JAX:012836) and maintained at the University of Edinburgh in a 12-h light/dark cycle under standard SPF conditions. Thy1-hTDP-43^{WT} overexpression mice were maintained on the mixed C57BL6/J × SJL background for comparison with the original description [23] unless otherwise stated. Mice were bred and handled in accordance with the University of Edinburgh and UK Home Office regulations, project licence number P92BB9F93. FVB mice were obtained from Charles River (RRID:IMSR_CRL:207) and crossed with heterozygous Thy1-hTDP-43 mice for five generations. Mice homozygous for the Thy1-hTDP-43^{WT} transgene (referred to as hTDP-43$^{Tg/Tg}$) were monitored daily for body weight and progressive muscle weakness and paralysis, as previously described [25]. Day of birth was considered P1. The clinical scoring for the progression of hindlimb weakness and paralysis is described in Table 1. A mouse was given a clinical score of the most severe point in any of the three categories. A score of 3 in any parameter represents the humane endpoint for this model. Mice reaching the humane endpoint were euthanised either by cervical dislocation or overdose of anaesthetic. Wild-type littermates were used as controls (NTg); heterozygous littermates were not used in this study. Tissue for western blot analysis was flash frozen and stored at −80°C. Spinal cords for immunohistochemistry were flushed from the vertebral column, and the lumbar section was removed as identified by the lumbar enlargement. Spinal cord sections were fixed in 4% paraformaldehyde overnight, dehydrated in 30% sucrose and embedded in OCT/sucrose for cryosectioning. Muscles dissected for immunohistochemistry were dissected and fixed in 4% paraformaldehyde for 30 min at room temperature and then stored in PBS. Large muscles such as TA, *extensor digitorum longus* (EDL), *peroneus longus* (PL), *peroneus brevis* (PB), GC, SOL and *plantaris* were micro-dissected into small bundles containing 10–20 muscle fibres, whereas flat muscles such as the cranial muscles and *transversus abdominis* (TVA) and small muscles such as the *lumbricals* and *flexor digitorum brevis* (FDB) were whole-mounted after clearing connective tissue.

Motor neuron immunohistochemistry

Spinal cords from lumbar segments L1–L3 were sectioned at 25-μm thickness. For motor neuron counts, sections were stained with NeuroTrace 500/525 (a fluorescent Nissl stain; N21480 ThermoFisher; 1:200 in PBS) and counter-stained with DAPI (4′,6-Diamidino-2-Phenylindole; ThermoFisher; 300 nM). Images of both ventral horns for two to three spinal cord sections per mouse were captured using a Nikon A1R confocal on a 20× objective. Motor neurons were counted as a cell width above 20 μm with an intense Nissl signal in the ventral horn. Thresholding the cell diameter at 20 μm limits the counts to alpha motor neurons only and excludes other motor neuron types. Total counts were averaged per ventral horn for comparison. Staining, imaging and analysis were performed by a researcher blinded to mouse genotype. For TDP-43 immunohistochemistry, sections underwent antigen retrieval in 10-mM citrate buffer, permeabilization in 0.5% Triton X-100 and incubation with the following primary antibodies: anti-ChAT (Millipore Cat# AB144P, RRID:AB_2079751) and anti-TDP-43 (Proteintech Cat# 10782-2-AP, RRID:AB_615042). Sections were then washed and probed with the following secondary antibodies: donkey anti-goat 594 (Thermo Fisher Scientific Cat# A-11058, RRID:AB_2534105) and donkey anti-rabbit 488 (Thermo Fisher Scientific Cat# A-21206, RRID:AB_2535792).

TABLE 1 Clinical scoring for hTDP-43$^{Tg/Tg}$ mouse model.

Score	Tail suspension	Grip test	Free movement
0	Both limbs consistently splayed outward	Mouse can grip the edge of a cup with both hind paws	Normal movement, weight supported on all limbs
1	One limb retracted towards the abdomen for more than 50% of the time	Mouse shows weakness in gripping with one hind paw	Mouse has a mild tremor or limp when walking
2	Both limbs are partially retracted towards the body for more than 50% of the time	Mouse shows weakness in gripping with both hind paws	Mouse shows severe tremor and/or limp, or the feet point away from the body during locomotion (‘duck feet’)
3	Both limbs are fully retracted for more than 50% of the time	Mouse cannot grip with either hind paw	Mouse has difficulty moving forward and drags its abdomen along the ground

Note: Mice are assigned a clinical score based on the most severe point in any category. A clinical score of 3 in any parameter is classified as the humane endpoint for this mouse model.

13652990, 2023, 4, Downloaded from https://onlinelibrary.wiley.com/doi/10.1111/nan.12925 by Universidade Estadual Paulista, Wiley Online Library on [24/09/2026]. See the Terms and Conditions (https://onlinelibrary.wiley.com/terms-and-conditions) on Wiley Online Library for rules of use; OA articles are governed by the applicable Creative Commons License

Neuromuscular junction immunohistochemistry

NMJs were labelled for presynaptic and postsynaptic components as previously described [26]. Muscles were incubated in 0.1 M glycine to reduce autofluorescence; tetramethyl-rhodamine isothiocyanate-conjugated α-bungarotoxin (TRITC α-BTX; VWR International Ltd) 1:500 to label AChRs; permeabilised in 4% Triton X-100 (2% Triton X-100 P8 tissue); blocked in 4% bovine serum albumin and 2% Triton X-100. Primary antibody incubation was performed over two nights at 4°C: rabbit anti-S100 (Agilent Cat# GA50461–2, RRID:AB_2811056) to label tSCs; mouse anti-SV2 and mouse anti 2H3 (DSHB Cat# SV2, RRID:AB_2315387; DSHB Cat# 2H3, RRID:AB_531793) to label synaptic vesicles and neurofilaments, respectively. Tissue was then incubated in the following secondary antibodies overnight at 4°C (Thermo Fisher Scientific Donkey anti-Mouse IgG (H + L) Highly Cross-Adsorbed Secondary Antibody, Alexa Fluor™ 488, Cat# A-21202, RRID:AB141607; Thermo Fisher Scientific Donkey anti-Rabbit IgG (H + L) Highly Cross-Adsorbed Secondary Antibody, Alexa Fluor™ 680, Cat# A10043, RRID:AB2534018, 1:500 dilution) and finally nuclear staining with DAPI (300 nM). Muscle fibres were mounted on a glass slide in Mowiol and stored at 4°C until imaging.

Neuromuscular junction imaging and quantification

A minimum of 40 *en face* NMJs per muscle were acquired using a Nikon A1R FLIM confocal laser scanning microscope with a 60×/1.4 oil immersion objective. Images were taken at 16-bit, 512 × 512-pixel frame size, Z-stack images with 0.5- to 1-μm interval, blue channel (405-nm excitation), green channel (488-nm excitation), red channel (561-nm excitation) and far-red channel (690-nm excitation). Maximum-intensity projection images were used for the analysis. Qualitative innervation analysis was performed visually by assessing the distance that the nerve terminal extends from where the axon enters the NMJ over the postsynaptic endplate.

NMJs were classified as 'fully innervated' (endplates fully covered by nerve terminals), 'vacant' (fully vacant endplates with no nerve coverage, i.e., completely denervated), or 'partially innervated'. Partial innervation is a qualitative category subjective to the investigator, where areas of endplate that would normally be associated with the nerve terminal are absent.

For tSC analysis, NMJs were classified as 'fully covered' (no loss of S100 labelling over the endplate) or 'uncovered' (with either partial or complete loss of S100 labelling over the endplate). And finally, to study the changes of presynaptic and postsynaptic elements, quantification analysis was performed using the automated version of NMJ-morph: aNMJ-morph [27, 28]. Nerve terminal 'complexity' was calculated as log10 (No. Terminal Branches × No. Branch Points × Total Length of Branches). Endplate 'compactness' was calculated as (AChR Area/Endplate Area) × 100. Endplate 'fragmentation' was calculated as 1 − (1/Number of AChR Clusters); the greater the number of clusters, the higher the fragmentation. The 'overlap' of presynaptic and postsynaptic structures was calculated as the area of synaptic contact/total area AChRs × 100. Percentage overlap is a quantitative measure directly comparable with the qualitative innervation analysis. However, qualitative innervation analysis is a subjective assessment of how far the nerve terminal extends over the endplate, whereas the quantitative NMJ-morph output calculates the number of pixels overlaid with red/green channels and will never be 100% because of the structure of the NMJ and spread of AChRs.

Western blotting

Whole spinal cords and whole brains were harvested, with the tissue homogenised in Pierce™ RIPA buffer (Thermo Fisher Cat# 89900) with protease inhibitor (Thermo Fisher Cat# 1861278), centrifuged, and the protein supernatant taken for western blotting. Total protein was measured using the Pierce™ BCA Protein Assay Kit (Thermo Fisher). Twenty micrograms of protein was loaded per lane on NuPAGE™ 4 to 12%, Bis-Tris Mini Protein Gels, transferred to PVDF membranes using iBlot 2 Transfer Device (Thermo Fisher) and stained with Revert 700 Total Protein Stain (LiCor). Probes for pan-TDP-43 (Proteintech Cat# 10782-2-AP, RRID:AB_615042) or human TDP-43 (Abnova Cat# H00023435-M01, RRID:AB_425904) and IR 800 secondary antibodies (LI-COR Biosciences Cat# 926-32213, RRID:AB_621848; LI-COR Biosciences Cat# 926-32212, RRID:AB_621847). The blots were imaged on a LiCOR Odyssey scanner, and the protein for each sample was quantified by normalising the signal against the Total Protein Stain (Figure S1).

Statistics

Statistics were performed using GraphPad Prism software version 9. Survival was plotted as Kaplan–Meier curves and compared using the Mantel–Cox test. Bars represent mean ± SEM unless otherwise stated. Statistical tests are described in figure legends.

RESULTS

Disease progression in the hTDP-43 mouse model

In order to better characterise the hTDP-43$^{Tg/Tg}$ mouse model, we first followed the progression of gross disease phenotypes across the lifespan. We monitored the progression of paralysis in hTDP-43$^{Tg/Tg}$ mice using clinical scores (Table 1; Figure 1B), with a clinical score of 3 in any parameter indicating the humane endpoint for this model. hTDP-43$^{Tg/Tg}$ mice represent a severe, rapidly progressing model of TDP-43 proteinopathy, as originally described [23], and had a median survival of 21 days (Figure 1A). hTDP-43$^{Tg/Tg}$ mice became

13652990, 2023, 4, Downloaded from https://onlinelibrary.wiley.com/doi/10.1111/nan.12925 by Universidade Estadual Paulista, Wiley Online Library on [24/09/2026]. See the Terms and Conditions (https://onlinelibrary.wiley.com/terms-and-conditions) on Wiley Online Library for rules of use; OA articles are governed by the applicable Creative Commons License

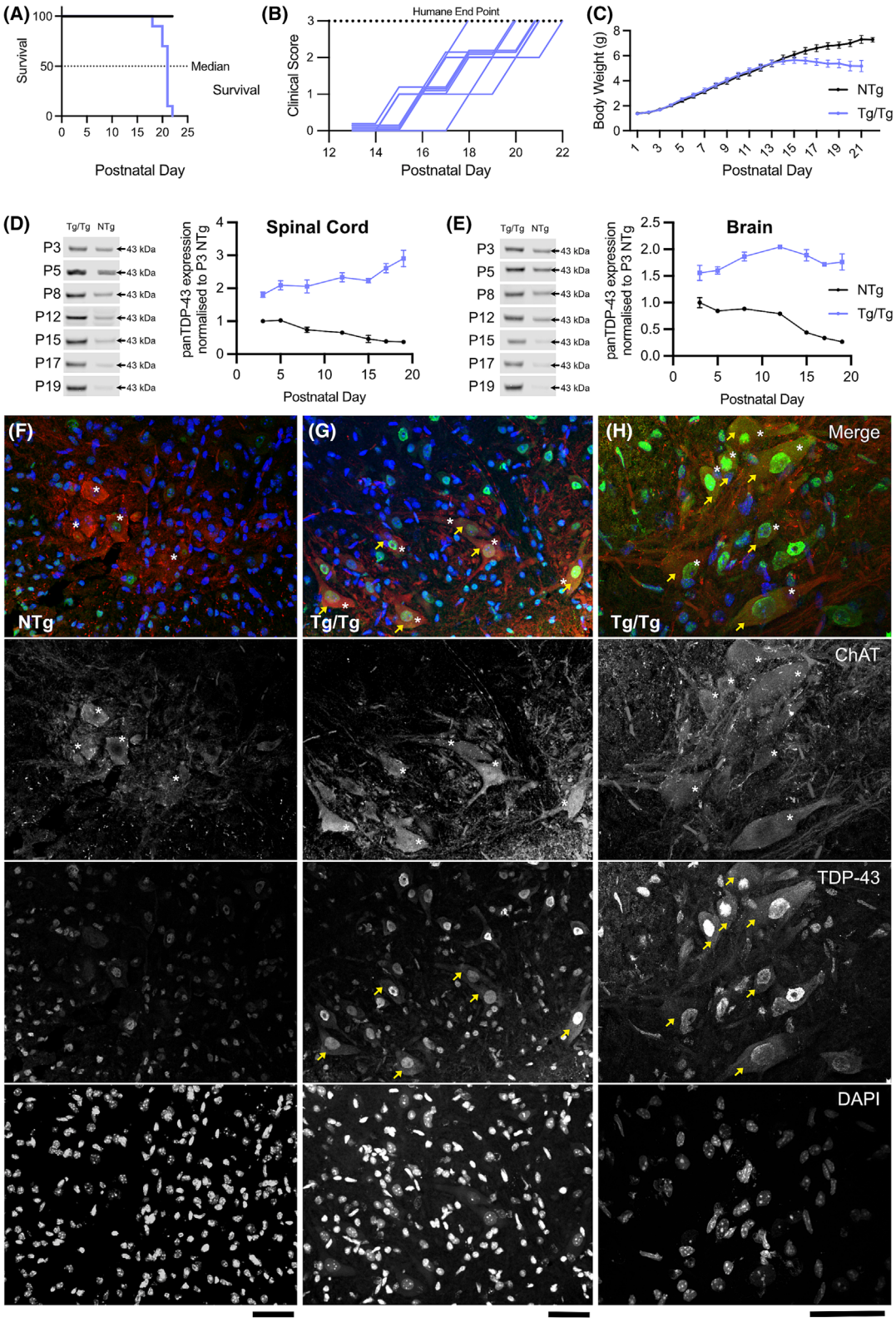


FIGURE 1 Legend on next page.

13652990, 2023, 4, Downloaded from https://onlinelibrary.wiley.com/doi/10.1111/nan.12925 by Universidade Estadual Paulista, Wiley Online Library on [24/09/2026]. See the Terms and Conditions (https://onlinelibrary.wiley.com/terms-and-conditions) on Wiley Online Library for rules of use; OA articles are governed by the applicable Creative Commons License

FIGURE 1 TDP-43 expression increases in the spinal cord and brain of the hTDP-43$^{Tg/Tg}$ mouse. (A) Kaplan–Meier curve of hTDP-43$^{Tg/Tg}$ mice reaching humane endpoint of clinical score 3 vs non-transgenic (NTg) mice, $n = 10$ per group. (B) Progressive clinical scores of hTDP-43$^{Tg/Tg}$ mice. Each line represents an individual mouse. (C) Body weights of hTDP-43$^{Tg/Tg}$ compared with NTg mice, $n = 10$ per group. (D) Western blots showing change of expression of TDP-43 in the spinal cord of hTDP-43$^{Tg/Tg}$ vs NTg mice over time, mean ± SEM, $n = 3$ per time point. (E) Western blots showing change of expression of TDP-43 in the brain of hTDP-43$^{Tg/Tg}$ vs NTg mice over time, mean ± SEM, $n = 3$ per time point. (F–H) Immunohistochemistry of spinal cord from (F) hTDP-43^{NTg} mouse (×20 magnification), (G) hTDP-43$^{Tg/Tg}$ mouse (×20 magnification), (H) hTDP-43$^{Tg/Tg}$ mouse (×60 magnification) choline acetyltransferase (ChAT), TDP-43 and DAPI. Stars indicate ChAT-positive motor neurons, and arrows indicate TDP-43 cytoplasmic localisation. Scale bars = 50 μm.

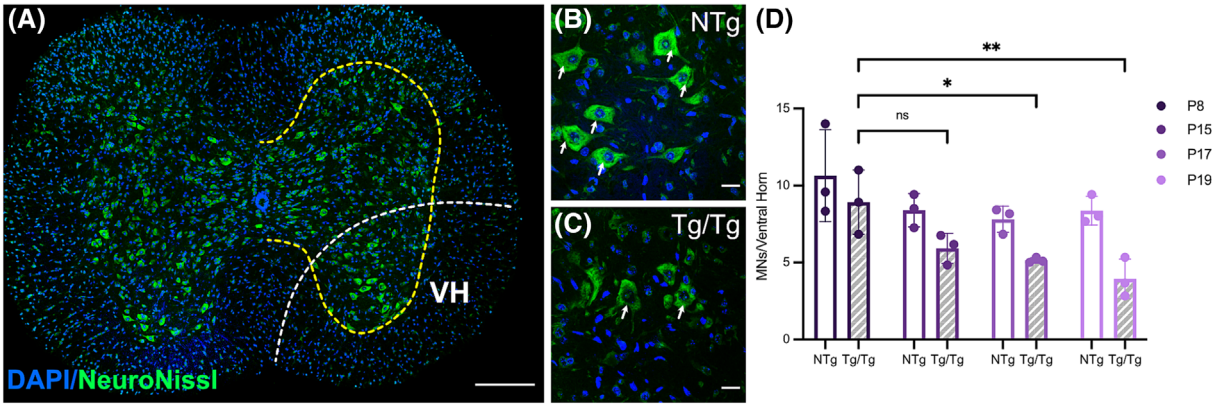


FIGURE 2 Significant motor neuron loss in the spinal cord of hTDP-43$^{Tg/Tg}$ mice from P17. (A) Example section of hTDP-43$^{Tg/Tg}$ mouse lumbar (L1–L3) spinal cord highlighting grey matter (yellow dotted line) and ventral horn (VH; white dotted line). Scale bars = 200 μm. Alpha-motor neurons were classified as being located in the ventral horn (VH) with a cell body of >20 μm. (B, C) Example images of ventral horn regions from hTDP-43$^{Tg/Tg}$ mouse (Tg/Tg) and littermate control (NTg). Scale bars = 20 μm; motor neurons indicated by white arrows. (D) Quantification of motor neurons per time point per genotype. Each point represents an average of six ventral horn sections from an individual mouse. Two-way ANOVA with Šidák's multiple comparisons test. ns, non-significant, * = $p < 0.05$, ** = $p < 0.01$.

distinguishable from control littermates at around 14 days, with the onset of progressive hindlimb paralysis and stabilisation, ultimately leading to a plateau of body weight compared with the weight gain observed in littermates (Figure 1C).

The hTDP-43 transgene in this model is under the Thy1 promoter, which is neuronal specific and increases in expression over the neonatal period [29]. We therefore sought to determine TDP-43 expression over time compared with non-transgenic littermate controls (NTg). Using a TDP-43 antibody that recognises both human and mouse protein, we could assess the expression of both endogenous TDP-43 and the transgene. At the earliest time point analysed, P3, there was already twice the amount of TDP-43 in the total spinal cord lysate of hTDP-43$^{Tg/Tg}$ mice (Figure 1D). TDP-43 expression continued to increase in hTDP-43$^{Tg/Tg}$ mice, until end-stage, where there was a 3-fold increase in the spinal cord compared with P3 NTg controls (Figure 1D). In comparison, there was decreasing expression of endogenous TDP-43 expression in the spinal cord of NTg controls (Figure 1D). We observed a lower overall expression of TDP-43 in total brain lysate of hTDP-43$^{Tg/Tg}$ mice that remained between 1.5- and 2-fold over NTg controls at P3 (Figure 1E). Using an antibody specific to human TDP-43 (i.e., the transgenic form), we confirmed the pattern of increasing expression from P3 onwards in both the brain and spinal cord compared with littermate controls (Figure S2). This increase in TDP-43 expression is evident in the nucleus and was also accompanied by the mislocalisation of TDP-43 to the cytoplasm of motor neurons at P19 (Figure 1F–H).

Motor neuron cell death begins at P15

Using a fluorescent Nissl stain, we quantified the number of alpha motor neurons in the ventral grey horn of the lumbar spinal cord (Figure 2A–C). Using four different time points (pre-symptomatic P8, early symptomatic P15, symptomatic P17 and late symptomatic P19), we determined that motor neuron loss in the lumbar spinal cord correlated with symptom progression. We found no significant difference in motor neuron number in hTDP-43$^{Tg/Tg}$ mice at P8 compared with NTg control ($p = 0.76$; Figure 2D). Motor neuron count began to decrease at the early symptomatic time point of P15 with a further decrease of nearly 50% compared with P8 NTg controls (5.92 ± 0.57 motor neurons per VH; $p < 0.05$), with motor neuron number further declining through symptomatic time points to only 3.94 ± 0.73 motor neurons in the ventral horn of P19 hTDP-43$^{Tg/Tg}$ mice ($p < 0.001$; Figure 2D).

13652990, 2023, 4, Downloaded from https://onlinelibrary.wiley.com/doi/10.1111/nan.12925 by Universidade Estadual Paulista, Wiley Online Library on [24/09/2026]. See the Terms and Conditions (https://onlinelibrary.wiley.com/terms-and-conditions) on Wiley Online Library for rules of use; OA articles are governed by the applicable Creative Commons License

hTDP-43 overexpression phenotype is not altered by the genetic background of mice

hTDP-43$^{Tg/Tg}$ mice were purchased from Jackson Labs on a C57BL/6JxSJL mixed genetic background. The background strain of a mouse model can have a dramatic impact on phenotype, for example, in a model of spinal muscular atrophy, where shifting the background strain changed the phenotype from a median lifespan of 5 days to being embryologically lethal [30]. Mixed background strains may therefore introduce an unnecessary element of variability, even within litters. We therefore crossed the hTDP-43 transgene onto the FVB background, a strain that is often used for transgenic line creation. After five generational crosses onto the FVB background, we compared clinical phenotypes and transgene expression between the FVB-hTDP-43$^{Tg/Tg}$ mice and the original C57BL/6J × SJL-hTDP-43$^{Tg/Tg}$ mice. FVB-hTDP-43$^{Tg/Tg}$ mice retained the severe ALS-like phenotype, with progressive muscle weakness leading to paralysis by day 22 (Figure S3A). FVB mice were on average larger than C57BL/6J mice, and this was observed in the FVB-hTDP-43$^{Tg/Tg}$ animals, which were significantly heavier than C57BL/6J × SJL-hTDP-43$^{Tg/Tg}$ animals from the pre-symptomatic time point P8 (Figure S3B). This increased body weight likely contributed to the modest increase in median survival of FVB-hTDP-43$^{Tg/Tg}$ mice (Figure S3A). Expression of the hTDP-43 transgene was not significantly different between FVB-hTDP-43$^{Tg/Tg}$ mice and C57BL/6J × SJL-hTDP-43$^{Tg/Tg}$ mice (Figure S3C–F). We therefore conclude that differences in background strain do not have a major impact on this TDP-43 overexpression model and that FVB-hTDP-43$^{Tg/Tg}$ mice can be used as an alternative to the mixed background C57BL/6J × SJL-hTDP-43$^{Tg/Tg}$ model where required.

Pronounced NMJ denervation in hindlimb muscles at end-stage

Denervation of the NMJ is a key pathological marker of motor neuron diseases [1, 6]. We therefore sought to characterise the pattern of denervation in different muscle groups across body regions of hTDP-43$^{Tg/Tg}$ mice, firstly at the end-stage of disease. When assessing NMJs, each NMJ was classified as either fully innervated (where the presynaptic neuron covered the entire endplate), partially innervated (between 20% and 80% of endplate covered by nerve terminal) or vacant (where there is an endplate without any presynaptic coverage). Muscles from four different regions were assessed for their denervation status: hindlimb muscles, forelimb muscles, trunk and cranial muscles. Hindlimb muscles (*lumbricals*, FDB, TA, EDL, PL, PB, SOL, GC, *plantaris*) showed the most pronounced denervation, with an average of 40% NMJs being fully innervated, whereas 25% of NMJs were vacant ($p < 0.01$; Figure 3A). By comparison, forelimb muscles (*lumbricals*) and trunk muscles (TVA) were not affected, with no significant increase in denervation (Figure 3C,D). Interestingly, cranial muscles (IS, LALr, LALc, AS, AAL) did show a mild denervation pattern, with ~5% NMJs being vacant ($p < 0.05$; Figure 3B).

NMJ denervation is seen in all muscle fibre types

Based on evidence from the SOD1 mouse models, fast-twitch muscle fibres are considered more vulnerable to disease, whereas slow-twitch muscle fibres are relatively resistant [15]. We therefore separately quantified NMJ denervation per muscle in the hindlimb and cranial muscles. We quantified pathological NMJs to be either partially denervated or fully vacant, as even partial denervation is exceptionally rare to observe in wild-type NMJs. Within the group of hindlimb muscles assessed, the most distal muscles, *lumbricals* and FDB, were significantly affected with 45.4% ($p < 0.0001$) and 78.8% ($p < 0.001$) pathological NMJs, respectively, compared with NTg controls (Figure 4A,C, representative images in Figure S4). The more proximal hindlimb muscles also showed significant denervation, with the fast-fibre type muscles TA and EDL showing a percentage of pathological NMJs of 34.6% and 33.7%, respectively ($p < 0.05$), whereas the mixed fibre type muscles PL, PB, GC and *plantaris* had 64.8%, 59.9%, 63.4% and 66.8% pathological NMJs, respectively ($p < 0.01$), although there was marked heterogeneity across animals (Figure 4A,C). The SOL muscle, mainly slow-twitch, showed a low degree of pathological NMJs at 24.3% ($p < 0.01$). By comparison, of the cranial muscles analysed, only the AS and IS showed a significant number of pathological NMJs (23.1% and 18.8%, respectively; $p < 0.05$), whereas the considerable degree of heterogeneity observed in the AAL, LALr and LALc obscured any significant differences (Figure 4B,D, representative images Figure S5). These trends of denervation are consistent with the analysis of vacant NMJs alone (Figure S6). These data show that all hindlimb muscles analysed display consistent denervation to some degree in hTDP-43$^{Tg/Tg}$ mice at end-stage. This is contrary to evidence from the SOD1 mouse, where NMJ denervation is pronounced in the fast-twitch muscle TA, whereas the slow-twitch SOL is fully innervated at symptomatic time points [13]. Denervation in other TDP-43 mouse models is variable (reviewed in [17]). For example, the inducible ΔNLS TDP-43 model was analysed after 11 weeks of TDP-43 mislocalisation and showed 80% denervation in the TA and 50% denervation in the SOL [31], whereas the knock-in human mutant TDP-43^{M337V} and TDP-43^{G298S} mouse models only showed around 5% denervation in the TA at >2 years of age [21]. Although the most affected muscles identified in our model—hindlimb FDBs and *lumbricals*—were not analysed in any of these other TDP-43 mice models, the clear evidence of TDP-43-driven denervation in the hTDP-43$^{Tg/Tg}$ mice makes it an important model of NMJ dysfunction.

Terminal Schwann cell pathology at end-stage

The third cellular component of the NMJ is the tSC, a non-myelinating Schwann cell type that is crucial for synapse development and maintenance [26]. In a healthy NMJ, tSCs are found overlying the motor neuron and muscle endplate, with an average of 1.7 tSCs per NMJ in mice [26]. tSCs are known to show pathology in ALS patient tissue, with reduced S100 staining and abnormal cytoplasmic projections

13652990, 2023, 4, Downloaded from https://onlinelibrary.wiley.com/doi/10.1111/nan.12925 by Universidade Estadual Paulista, Wiley Online Library on [24/09/2026]. See the Terms and Conditions (https://onlinelibrary.wiley.com/terms-and-conditions) on Wiley Online Library for rules of use; OA articles are governed by the applicable Creative Commons License

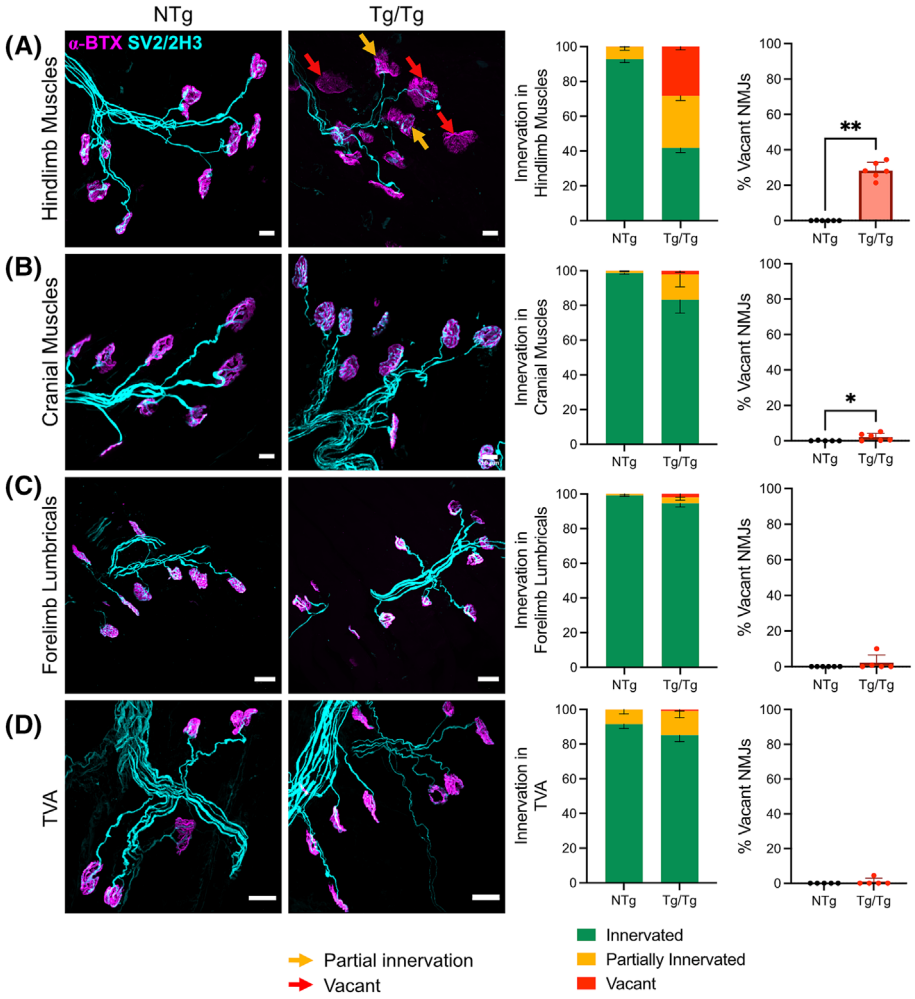


FIGURE 3 Regional denervation assessment in the hTDP-43$^{Tg/Tg}$ mouse at end-stage shows pronounced denervation in hindlimb muscles. Bar charts show the percentage of NMJs as an arithmetic mean from the pooled muscles of (A) hindlimb muscles and (B) cranial muscles and from (C) forepaw lumbricals and (D) TVA muscles. Bar charts quantifying the degree of endplate innervation (% fully innervated, % partially innervated, % vacant). The accompanying charts (% vacant NMJs) are averages ± SEM. Data points represent the pooled muscles from one animal, $N = 5$ animals, Mann–Whitney test, * = $p < 0.05$, ** = $p < 0.01$. Representative confocal images of muscle samples NTg and Tg/Tg NMJs from the corresponding body region. Endplates are labelled by α-bungarotoxin (magenta); nerve terminals and axons are labelled by anti-SV2 and anti-2H3 antibodies, respectively (cyan). Partially innervated NMJs are indicated by yellow arrows, and vacant NMJs are indicated by red arrows. Scale bars are 10 μm in hindlimb and cranial muscles and 20 μm in forepaw lumbricals and TVA.

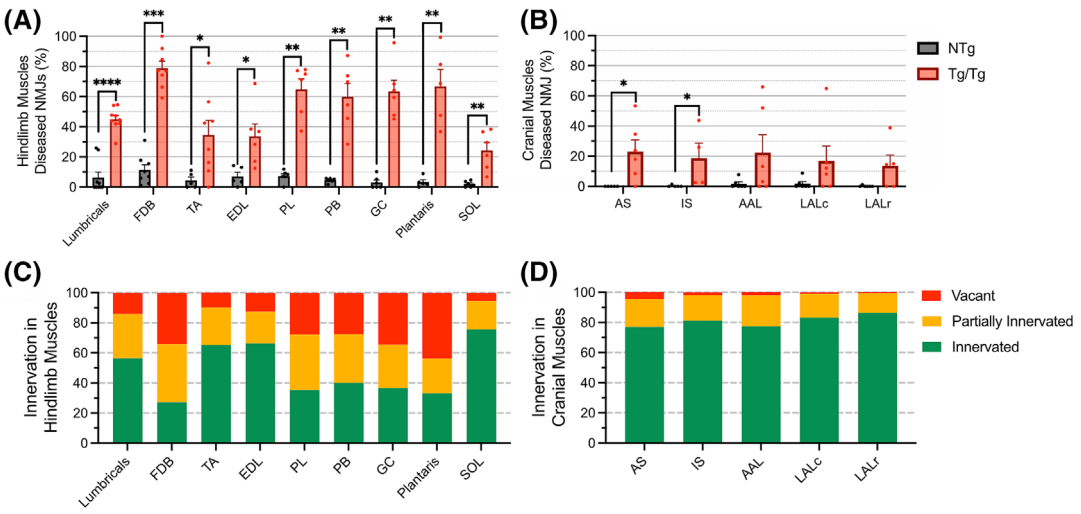


FIGURE 4 Denervation assessment of individual hindlimb and cranial muscles shows significant denervation across all types of muscle at end-stage in the hTDP-43$^{Tg/Tg}$ mouse. (A) Percentage of diseased NMJs (partially innervated and vacant combined) in each hindlimb muscle. (B) Percentage of diseased NMJs (partially innervated and vacant combined) in each cranial muscle. Points indicate a minimum of 30 NMJs per animal, average ± SEM, $n = 6–8$ animals. Mann–Whitney test, * = $p < 0.05$, ** = $p < 0.01$, *** = $p < 0.001$, **** = $p < 0.0001$. (C, D) Breakdown of innervation per muscle group in hindlimb and cranial muscles, respectively. FDB, flexor digitorum brevis; TA, tibialis anterior; EDL, extensor digitorum longus; PL, peroneus longus; PB, peroneus brevis; GC, gastrocnemius; SOL, soleus.

13652990, 2023, 4, Downloaded from https://onlinelibrary.wiley.com/doi/10.1111/nan.12925 by Universidade Estadual Paulista, Wiley Online Library on [24/09/2026]. See the Terms and Conditions (https://onlinelibrary.wiley.com/terms-and-conditions) on Wiley Online Library for rules of use; OA articles are governed by the applicable Creative Commons License

[32, 33], as well as in SOD1 mouse models [13, 34]. We therefore used an S100 antibody to assess tSC morphology in hTDP-43$^{Tg/Tg}$ mice at end-stage. The pattern of tSC coverage as indicated by S100 staining was similar to the pattern of denervation described above. Hindlimb muscles such as GC and *plantaris* showed substantial loss of S100 staining (Figure 5A–C), with 50% of NMJs from hindlimb muscles losing their tSC coverage either partially or completely (Figure 5E); in contrast, cranial muscles did not show any loss of S100

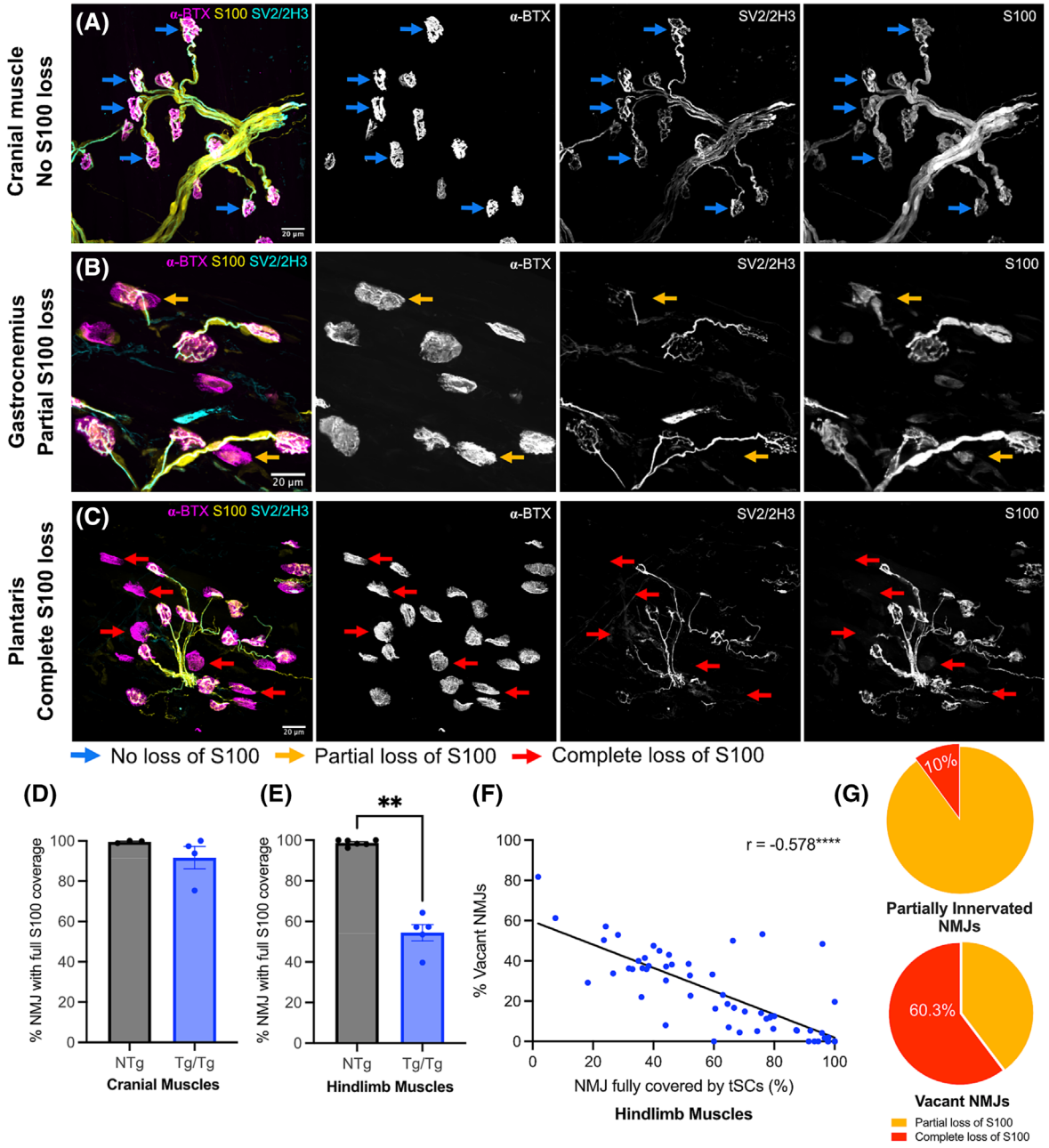


FIGURE 5 Terminal Schwann cell loss in hTDP-43$^{Tg/Tg}$ mice correlates with denervation at end-stage. Representative confocal micrographs of hTDP-43$^{Tg/Tg}$ mouse NMJs from (A) cranial muscles, (B) gastrocnemius and (C) plantaris at disease end-stage with S100 labelling for terminal Schwann cells. Red arrows indicate complete loss of the S100. Blue arrows indicate complete labelling of the S100. Orange arrows indicate partial loss of the S100 labelling. Endplates are labelled by α-bungarotoxin (magenta); nerve terminals and axons are labelled by anti-SV2 and anti-2H3 antibodies, respectively (cyan). tSCs are labelled by anti S100 (yellow). Scale bars = 20 µm in all images. (D, E) Percentage of NMJs that are fully covered by tSCs in pooled cranial and hindlimb muscles. Each data point represents the mean values of all pooled cranial or hindlimb muscles from one animal, a minimum of 30 NMJs per animal. (F) Strong negative correlation between the percentage of vacant NMJs and percentage of NMJs covered by tSCs in hindlimb muscles of five hTDP-43$^{Tg/Tg}$ animals at disease end-stage. Each data point represents one hindlimb muscle, simple linear regression, slope = −0.578, $p < 0.0001$. (G) Pie charts show that the vast majority of partially innervated NMJs were partially covered by tSCs (90%), whereas more than 60% of vacant NMJs have completely lost their tSCs coverage.

13652990, 2023, 4, Downloaded from https://onlinelibrary.wiley.com/doi/10.1111/nan.12925 by Universidade Estadual Paulista, Wiley Online Library on [24/09/2026]. See the Terms and Conditions (https://onlinelibrary.wiley.com/terms-and-conditions) on Wiley Online Library for rules of use; OA articles are governed by the applicable Creative Commons License

TABLE 2 Morphological analysis of NMJs in the hindlimb muscles of hTDP-43$^{Tg/Tg}$ mice vs NTg control using aNMJ morph.

Morphometrical variables		*Lumbricals*		*TA*		*PB*		*PL*	
		NTg	hTDP-43$^{Tg/Tg}$	NTg	hTDP-43$^{Tg/Tg}$	NTg	hTDP-43$^{Tg/Tg}$	NTg	hTDP-43$^{Tg/Tg}$
Presynaptic variables	Axon diameter (μm)	0.96 ± 0.14	**0.40 ± 0.04****	1.06 ± 0.08	**0.60 ± 0.08****	0.76 ± 0.09	**0.28 ± 0.06****	0.86 ± 0.11	**0.23 ± 0.07*****
	NT area (μm^2)	80.9 ± 8.8	**37.1 ± 5.5****	83.9 ± 5.7	72.7 ± 13.8	74.7 ± 3.6	**29.7 ± 5.3*****	73.2 ± 5.4	**37.7 ± 7.8****
	NT perimeter (μm)	110.6 ± 7.9	**68.3 ± 4.5****	134.7 ± 9.2	130 ± 22.5	111.6 ± 3.3	**54.5 ± 11.8*****	108.2 ± 5.5	**63.0 ± 9.0****
	NT complexity	3.3 ± 0.2	3.1 ± 0.1	3.6 ± 0.1	3.4 ± 0.4	3.3 ± 0.1	2.6 ± 0.3	3.2 ± 0.1	**2.4 ± 0.2****
Postsynaptic variables	AChR area (μm^2)	146.8 ± 17.6	132.7 ± 23.5	163.7 ± 49.6	170.4 ± 69.0	138.5 ± 11.8	157.9 ± 30.2	142.9 ± 28.5	152.3 ± 24.7
	Endplate area (μm^2)	241.5 ± 26.8	205.7 ± 27.4	273.5 ± 57.4	288.8 ± 83.8	213.9 ± 23.3	237.3 ± 46.3	224.1 ± 38.1	234.6 ± 58.7
	Compactness (%)	61.0 ± 1.8	63.8 ± 2.0	59.0 ± 2.5	57.5 ± 4.4	64.3 ± 0.8	65.8 ± 1.1	63.2 ± 0.9	66.6 ± 1.7
	AChR cluster number	1.02 ± 0.02	1.05 ± 0.03	1.05 ± 0.04	1.1 ± 0.06	0.98 ± 0.03	0.95 ± 0.04	0.99 ± 0.02	1.00 ± 0.06
	Fragmentation	0.02 ± 0.01	0.03 ± 0.01	0.03 ± 0.02	0.08 ± 0.04	0.02 ± 0.01	0.02 ± 0.01	0.01 ± 0.00	0.03 ± 0.01
Others	Overlap (%)	43.6 ± 4.3	**21.7 ± 2.3***	44.0 ± 1.4	32.6 ± 4.7	48.4 ± 1.3	**16.5 ± 3.3****	44.3 ± 1.4	**17.8 ± 2.5****

Note: Values are the mean of 40–60 NMJs per animal ± SEM, $N = 6$–8 animals. *T*-test comparison: axon diameter, NT area, AChR area, NT perimeter, endplate area. Mann–Whitney comparison: fragmentation, compactness, overlap, complexity, cluster number.

Abbreviations: TA, *tibialis anterior*; PB, *peroneus brevis*; PL, *peroneus longus*; SOL, *soleus*; GC, *gastrocnemius*; NT, nerve terminals; AChR, acetylcholine receptors.

*$p < 0.05$.

**$p < 0.01$.

***$p < 0.001$.

****$p < 0.0001$.

13652990, 2023, 4, Downloaded from https://onlinelibrary.wiley.com/doi/10.1111/nan.12925 by Universidade Estadual Paulista, Wiley Online Library on [24/09/2026]. See the Terms and Conditions (https://onlinelibrary.wiley.com/terms-and-conditions) on Wiley Online Library for rules of use; OA articles are governed by the applicable Creative Commons License

TABLE 2 (Continued)

Morphometrical variables	*SOL*		*GC*		*Plantaris*	
	NTg	hTDP-43$^{Tg/Tg}$	NTg	hTDP-43$^{Tg/Tg}$	NTg	hTDP-43$^{Tg/Tg}$
Presynaptic variables	1.03 ± 0.12	0.7 ± 0.05*	0.78 ± 0.03	0.24 ± 0.06**	0.79 ± 0.06	0.23 ± 0.06***
	88.3 ± 5.8	64.6 ± 4.5**	79.4 ± 4.0	33.7 ± 6.5***	65.7 ± 2.2	23.3 ± 5.5****
	108.3 ± 3.0	89.6 ± 5.0**	129.9 ± 5.6	65.17 ± 14.5**	110 ± 8.9	40.2 ± 8.3***
	3.4 ± 0.1	3.2 ± 0.2	3.68 ± 0.1	3.08 ± 0.3	3.2 ± 0.1	2.0 ± 0.2**
Postsynaptic variables	141.6 ± 15.1	147.8 ± 19.4	163.9 ± 26.5	180.6 ± 40.7	128.9 ± 20.1	134.1 ± 13.4
	230.0 ± 38.2	238.6 ± 34.3	244.7 ± 41.1	261.1 ± 65.3	210.2 ± 12.9	203.1 ± 20.5
	62.8 ± 2.1	63.0 ± 1.7	66.9 ± 1.1	68.8 ± 1.8	63.6 ± 1.0	65.3 ± 0.8
	0.97 ± 0.03	1.01 ± 0.03	1.0 ± 0.04	0.99 ± 0.02	0.99 ± 0.06	0.93 ± 0.02
	0.03 ± 0.01	0.04 ± 0.01	0.02 ± 0.01	0.02 ± 0.00	0.03 ± 0.01	0.01 ± 0.00
Others	51.2 ± 1.3	36.3 ± 4.1*	43.9 ± 2.8	17.2 ± 2.0**	44.6 ± 1.5	14.2 ± 3.9**

Note: Values are the mean of 40–60 NMJs per animal ± SEM, $N = 6–8$ animals. *T*-test comparison: axon diameter, NT area, AChR area, NT perimeter, endplate area. Mann–Whitney comparison: fragmentation, compactness, overlap, complexity, cluster number.

Abbreviations: TA, *tibialis anterior*; PB, *peroneus brevis*; PL, *peroneus longus*; SOL, *soleus*; GC, *gastrocnemius*; NT, nerve terminals; AChR, acetylcholine receptors.

*$p < 0.05$.

**$p < 0.01$.

***$p < 0.001$.

****$p < 0.0001$.

13652990, 2023, 4, Downloaded from https://onlinelibrary.wiley.com/doi/10.1111/nan.12925 by Universidade Estadual Paulista, Wiley Online Library on [24/09/2026]. See the Terms and Conditions (https://onlinelibrary.wiley.com/terms-and-conditions) on Wiley Online Library for rules of use; OA articles are governed by the applicable Creative Commons License

staining ($p = 0.26$; Figure 5D). When examining the NMJs that showed a loss of S100 staining, we noted a correlation between those that were denervated and those that had a loss of S100 staining. Linear regression showed a strong negative correlation ($r = -0.578$) between % denervation and % coverage of tSCs ($p < 0.0001$; Figure 5F) (as NMJ denervation increases, tSC coverage decreases). Out of the vacant NMJs, 60.3% showed a complete loss of S100 staining, and the remaining showed a partial loss. In contrast, partially innervated NMJs showed partial S100 staining, with only 10% of partially innervated NMJs showing a complete loss of S100 (Figure 5G).

Presynaptic morphological changes at the NMJ

A more detailed assessment of the morphological changes occurring at the NMJ was made using NMJ-morph. NMJ-morph is a semi-automated ImageJ plug-in that allows quantitative assessment of several presynaptic and postsynaptic variables at the NMJ, providing a detailed and objective approach to NMJ assessment [27, 28, 35]. NMJs from the seven hindlimb muscles were analysed using NMJ-morph. In general, presynaptic variables such as nerve terminal area and axon diameter were significantly altered in hTDP-43$^{Tg/Tg}$ mice, whereas no changes were observed in postsynaptic variables such as endplate area and fragmentation, between hTDP-43$^{Tg/Tg}$ mice and NTg controls (Table 2). This distinction between presynaptic and postsynaptic changes highlights the motor neuron-specific nature of this model. The percentage 'overlap' between the presynaptic and postsynaptic components of the NMJ provides an exact measurement of the degree of synaptic contact between nerve terminal and endplate (and thus innervation). Because this approach measures the number of overlapping pixels from presynaptic and postsynaptic structures, fully innervated NMJs from wild-type mice are calculated to have an overlap of 40%–50% (Table 2) in keeping with previous reports [35]. Importantly, this overlap is consistent over the whole NMJ (Figure 3). This value is therefore not to be confused with the qualitative assessment of denervation described previously, which considers partially denervated NMJs to be those where at least 30% of the whole endplate is not in contact with an associated nerve terminal, being partially vacant. Here, we found that quantitative assessment of overlap of the NMJ shows the same trends as the qualitative denervation assessment, where there was a significant decrease in overlap (indicating denervation) in all hindlimb muscles analysed except for the TA, where there was a high degree of variation (Table 2).

Quantification of the presynaptic variable 'nerve terminal area' is shown in Figure 6A. Interestingly, changes in the nerve terminal area did not entirely correlate with the degree of denervation. Although PB and *plantaris* muscles continued to be most affected in hTDP-43$^{Tg/Tg}$ mice followed by PL, GC and *lumbricals*, SOL also showed a significant decrease in nerve terminal area, whereas the TA was not significantly affected (Figure 6A). In contrast, the postsynaptic variable of the AChR area was not significantly changed in any of the muscles analysed (Figure 6B).

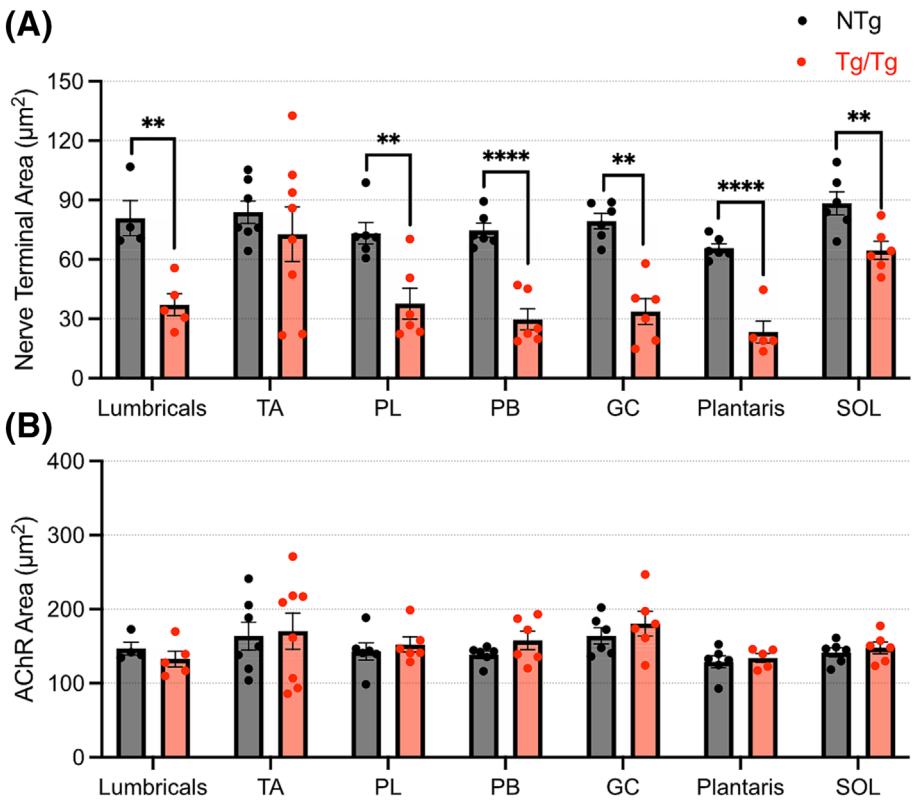


FIGURE 6 aNMJ-morph analysis of hindlimb muscles shows pathology in the presynaptic but not postsynaptic compartment. (A) Example presynaptic variable (nerve terminal area) comparing non-transgenic littermates (NTg) with hTDP-43$^{Tg/Tg}$ mice (Tg/Tg). (B) Example postsynaptic variable (acetylcholine receptor area) comparing non-transgenic littermates (NTg) with hTDP-43$^{Tg/Tg}$ mice (Tg/Tg). TA, tibialis anterior; PL, peroneus longus; PB, peroneus brevis; GC, gastrocnemius; SOL, soleus. Points indicate a minimum of 40 NMJs per animal, average ± SEM, $n = 3$–8 animals. *T*-test comparisons, ** = $p < 0.01$, **** = $p < 0.0001$.

13652990, 2023, 4, Downloaded from https://onlinelibrary.wiley.com/doi/10.1111/nan.12925 by Universidade Estadual Paulista, Wiley Online Library on [24/09/2026]. See the Terms and Conditions (https://onlinelibrary.wiley.com/terms-and-conditions) on Wiley Online Library for rules of use; OA articles are governed by the applicable Creative Commons License

NMJ denervation begins at early symptomatic stages

In order to establish the time course of NMJ denervation in hTDP-43$^{Tg/Tg}$ mice, NMJ denervation was assessed in the severely affected muscles PL and *plantaris* as well as the least-affected muscle SOL over 3 time points—pre-symptomatic (P8), early symptomatic (P15) and end-stage (P19) (Figure 7). There was no denervation evident at the earliest time point P8 in any of the muscles analysed (Figure 7B). At the early symptomatic time point P15, the *plantaris* muscle showed 10% denervation (Figure 7A,B), whereas there was no change in innervation for the PL and SOL muscles (Figure 7B).

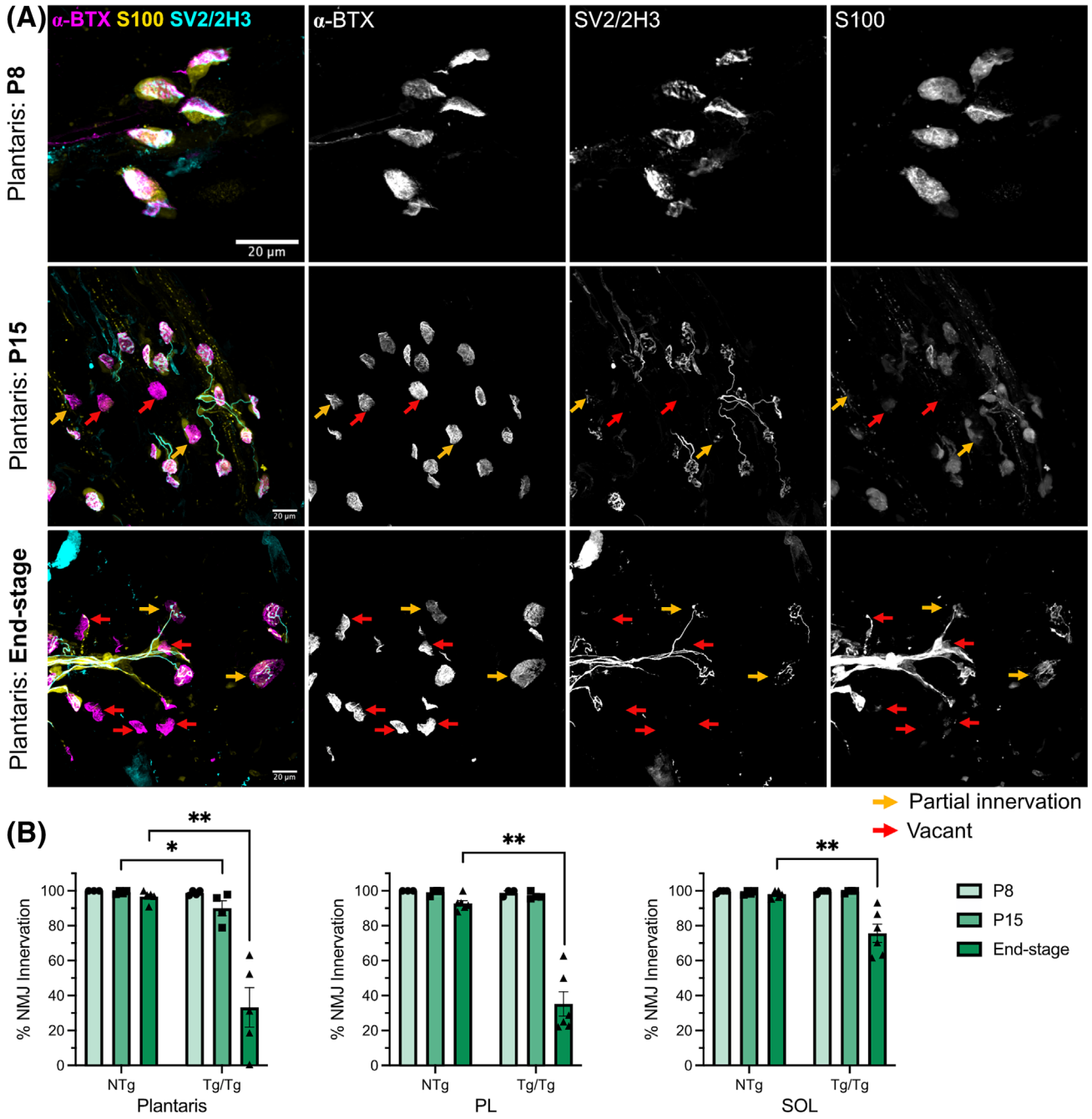


FIGURE 7 Innervation analysis at earlier time points shows denervation in *plantaris* muscle at an early symptomatic time point. (A) Representative confocal micrographs of *plantaris* NMJs in hTDP-43$^{Tg/Tg}$ mice at different time points: pre-symptomatic (P8), early symptomatic (P15) and at disease end-stage. Scale bars = 20 µm in all images. (B) Quantification of % innervation per time point, points indicate average % NMJ innervation per individual animal, minimum 30 NMJs per animal. Bars are averages ± SEM. Mann–Whitney test, * = $p < 0.05$, ** = $p < 0.01$.

13625990, 2023, 4, Downloaded from https://onlinelibrary.wiley.com/doi/10.1111/nan.12925 by Universidade Estadual Paulista, Wiley Online Library on [24/09/2026]. See the Terms and Conditions (https://onlinelibrary.wiley.com/terms-and-conditions) on Wiley Online Library for rules of use; OA articles are governed by the applicable Creative Commons License

DISCUSSION

Modelling motor neuron cell death and the accompanying NMJ dysfunction underlying ALS is difficult because of the complex genetic background, yet vital in terms of further understanding disease pathogenesis and developing drug therapies for patients. Here, we have presented a systematic analysis of pathology seen in the severe ALS mouse model Thy1-hTDP-43^{WT}, which recapitulates many aspects of ALS seen in human patients including progressive paralysis, muscle weakness and weight loss. Furthermore, we demonstrate recapitulation of many key aspects of pathology seen in ALS, including loss of motor neurons, progressive denervation at the NMJ, loss of tSCs from the NMJ and accumulation of cytoplasmic TDP-43.

TDP-43 is an RNA-binding protein that plays a role in the splicing of thousands of RNA transcripts [36]. Although there are more than 40 rare ALS-associated mutations found in the *TARDBP* gene encoding the TDP-43 protein [37], pathological TDP-43-positive inclusions are found in neurons of over 95% of ALS patients [5, 18]. Indeed, pathological inclusions are the same in sporadic cases with or without a mutation in *TARDBP* [19]. Importantly, we have confirmed cytoplasmic mislocalisation of TDP-43 in the Thy1-hTDP-43^{WT} model. These mice overexpress human 'wild-type' TDP-43 at a supraphysiological level rather than expressing one of the rare mutant forms of TDP-43. ALS arising from TDP-43 mutations accounts for a very small proportion of patients [38, 39], and so a toxic gain-of-function from mutant TDP-43 may not be applicable to the rest of the patient population. Instead, 'wild-type' TDP-43 is dysregulated through as-yet-unknown mechanisms, which is modelled here through increased expression. TDP-43 is essential for development, because *Tardbp*$^{-/-}$ embryos die at early embryonic stages, and is expressed throughout embryogenesis into adulthood [40, 41]. Our data confirm previous reports that expression of TDP-43 decreases over time in non-transgenic mice during postnatal development. Thy1-hTDP-43^{WT} mice showed slowly increasing expression of TDP-43 in both the brain and spinal cord in line with known *Thy1* promoter activity [29], apparently overwhelming the TDP-43 autoregulatory machinery [42], reaching a 3-fold increase in TDP-43 at endstage compared with NTg P3 controls. However, although there was increased TDP-43 expression at all time points measured, Thy1-hTDP-43^{WT} mice did not develop muscle weakness until P14, implying a threshold of tolerance for TDP-43 dysregulation. This correlated with the timeline of motor neuron cell death, where we found significantly fewer motor neurons Thy1-hTDP-43^{WT} spinal cord from P15 onwards. As well as a common phenotype across various forms of ALS, TDP-43 pathology is found in other neurodegenerative diseases such as frontotemporal lobar degeneration (FTLD), including behavioural variant frontotemporal dementia, and limbic-predominant age-related TDP-43 encephalopathy neuropathologic change (LATE-NC) with and without Alzheimer's disease [43, 44]. FTLD-TDP and ALS are considered to be on a spectrum because of their overlapping TDP-43 pathology and clinical presentation [45], and so, although we have focussed on describing motor neuron-related pathology here, this model may also be of interest for studying other TDP-43 proteinopathies.

Denervation at the NMJ is a critical component of motor neuron disease pathology. A key study into the progression of ALS pathology examined a patient who, having been evaluated in the clinic for ALS-like symptoms, died unexpectedly 2 weeks later of an unrelated cause [46]. This patient had shown evidence of denervation following electromyographic examination but demonstrated no overt neuronal loss in the spinal cord on post-mortem examination. This rare insight into early ALS pathology implies that distal regions of the motor axons and the NMJ are involved at the beginning of the cascade of events leading to motor neuron cell death, supporting the so-called 'dying-back hypothesis'. Here, we show in the Thy1-hTDP-43^{WT} mice that denervation is similarly observed at early symptomatic time points, alongside the earliest evidence of motor neuron loss. Denervation in this model was pronounced in distal muscles (*lumbricals*, FDB), with statistically significant differences in denervation between NTg and Tg/Tg mice observed in all hindlimb muscles assessed, whereas the trunk muscle (TVA) and forelimb *lumbricals* were not affected, and only a small degree of denervation was observed in cranial muscles. This model therefore mimics common presentations of ALS where distal muscles are the first to be affected [47]. Interestingly, although it is known that the subclass of fast-fatigable muscles in SOD1 mice are the first to be affected [48], here we show similar denervation patterns between the fast-fatigable TA and the slow-twitch SOL. It therefore seems that in this TDP-43-driven model, a vulnerability pattern of distal muscles compared with proximal muscles is more pronounced than any pattern regarding fibre type.

Because *Thy1* drives *hTDP-43* transgene expression from around day of birth, and the Tg/Tg mice showed significantly heightened expression as early as P3, TDP-43 overexpression is present in our model during the postnatal NMJ maturation period [49, 50]. We therefore cannot discount an influence of hTDP-43 overexpression on the normal developmental maturation of the NMJ alongside the observed contribution to denervation and motor neuron death. We did not observe any NMJ denervation until behavioural symptoms were observed (at P15), but there may be subtle changes to the NMJ at earlier stages that remained undetected. Regardless, this model, showing early and severe motor neuron pathology represents an important in vivo tool for ALS research, as it reduces the timeline required for experiments compared to longer-lived, less severe ALS models, such as the SOD1^{G93A} mouse. Although the first loss of MNs occurred around P15, not all muscles displayed NMJ denervation at P15. It remains unresolved, therefore, whether the MNs lost from the spinal cord correlate directly with the loss of NMJs in the earliest affected muscles. It is clear, however, that not all MNs and NMJs degenerate at the same time in this model, reflecting the consistent finding of differential motor unit vulnerability in ALS patients and rodent models.

We used the ImageJ-based workflow 'NMJ-morph' to quantitatively analyse presynaptic and postsynaptic features of the NMJs in hindlimb muscles. Traditionally, denervation has been determined by qualitative assessment of NMJs, as was performed in Figures 3 and 4. However, this subjective methodology is reliant on a consistent

13652990, 2023, 4, Downloaded from https://onlinelibrary.wiley.com/doi/10.1111/nan.12925 by Universidade Estadual Paulista, Wiley Online Library on [24/09/2026]. See the Terms and Conditions (https://onlinelibrary.wiley.com/terms-and-conditions) on Wiley Online Library for rules of use; OA articles are governed by the applicable Creative Commons License

approach between researchers, which is difficult to achieve in practise. NMJ-morph therefore represents a potentially powerful tool for motor neuron disease research, providing deeper insight into pathological features of the NMJ in a more reproducible manner than traditional simple denervation counts that are subject to investigator bias [27, 35, 51]. For example, NMJ-morph highlighted that the NMJ changes manifested in Thy1-hTDP-43^{WT} mice are found solely on the presynaptic (motor neuron) side of the NMJ, with significant changes in presynaptic variables such as axon diameter and nerve terminal area, whereas postsynaptic variables such as AChR area or number of AChR clusters were unchanged compared with wild-type controls. Because the transgene is expressed under a neuron-specific promoter, expression of TDP-43 in muscle was unchanged. These NMJs therefore model defects solely driven by pathological neuronal influence. Although it is unlikely that ALS pathology is restricted to motor neurons and that muscle-restricted expression of mutant SOD1 protein alone is sufficient to cause motor neuron degeneration [52], this simplified model of TDP-43-related NMJ denervation represents a powerful model system to study motor neuron-derived pathology at the NMJ.

As the third element of the tripartite NMJ, tSCs offer support to the presynaptic compartment and motor endplate [7]. tSCs are especially important following nerve injury, where they extend projections between denervated and innervated NMJs allowing re-innervation [53]. Sprouting, and therefore re-innervation, is deficient in the SOD1 ALS mouse model, particularly in fast-fatigable muscle [48]. Here, we reported a loss in S100-positive tSCs in the vulnerable hindlimb muscles of the Thy1-hTDP-43^{WT} mice but no change in tSC coverage of the NMJs in the cranial muscles. Importantly, we show that the coverage of the NMJ by tSCs had a significant negative correlation with the percentage of denervation in each muscle. Understanding the role of tSCs and the point at which they are lost in the sequence of pathology could be crucial to further understand ALS and other neuromuscular pathologies. Our work suggests that Thy1-hTDP-43^{WT} mice represent an ideal model system for such studies.

The Thy1-hTDP-43^{WT} mouse model provides a much-needed platform in ALS research, with significant ALS-associated phenotypes of motor neuron loss and NMJ denervation in a model that is not reliant on SOD1 mutations. Although severe, another facet to the Thy1-hTDP-43^{WT} mouse model is that the phenotype takes weeks to develop, rather than months or years, allowing for more rapid drug discovery that is so desperately needed by ALS patients. This model will therefore provide a powerful tool in future research for examining the crucial role of NMJ denervation in ALS progression both at the molecular level and as a drug target.

AUTHOR CONTRIBUTIONS

This project was administered by Helena Chaytow and Thomas H. Gillingwater. Helena Chaytow, Thomas H. Gillingwater, Ross A. Jones and Kiterie M. E. Faller conceived, planned and supervised these experiments. Abrar Alhindi, Megan Shand, Hannah L. Smith, Ana S. Leite, Yu-Ting Huang, Dinja van der Hoorn and Zara Ridgway conducted laboratory experiments. Abrar Alhindi, Megan Shand and Hannah L. Smith performed data analysis. Abrar Alhindi, Hannah L. Smith, Ross A. Jones, Thomas H. Gillingwater and Helena Chaytow wrote, reviewed and edited the original draft. All authors have read, reviewed and approved the final version of this paper.

ACKNOWLEDGEMENTS

The authors would like to thank the animal husbandry staff for their contribution to this work. This work was funded by PhD funding from King Abdulaziz University through the Saudi Cultural Bureau, London (to A.A.) and project grant funding from MND Scotland and the My Name'5 Doddie Foundation.

CONFLICT OF INTEREST STATEMENT

T.H.G. has served as an advisor for LifeArc, Neurogene, Roche and Novartis.

ETHICS STATEMENT

All animal work was performed in accordance with the University of Edinburgh and UK Home Office regulations, project licence number P92BB9F93.

PEER REVIEW

The peer review history for this article is available at https://www.webofscience.com/api/gateway/wos/peer-review/10.1111/nan.12925.

DATA AVAILABILITY STATEMENT

Datasets used in the current study are available from the corresponding author upon request.

ORCID

Helena Chaytow https://orcid.org/0000-0003-2257-7620

REFERENCES

1. van Es MA, Hardiman O, Chio A, et al. Amyotrophic lateral sclerosis. *Lancet*. 2017;390(10107):2084-2098. doi:10.1016/S0140-6736(17)31287-4
2. Zou ZY, Zhou ZR, Che CH, Liu CY, He RL, Huang HP. Genetic epidemiology of amyotrophic lateral sclerosis: a systematic review and meta-analysis. *J Neurol Neurosurg Psychiatry*. 2017;88(7):540-549. doi:10.1136/jnnp-2016-315018
3. Sleigh JN, Tosolini AP, Gordon D, et al. Mice carrying ALS mutant TDP-43, but not mutant FUS, display in vivo defects in axonal transport of signaling endosomes. *Cell Rep*. 2020;30(11):3655-3662.e2. doi:10.1016/j.celrep.2020.02.078
4. Arnold ES, Ling SC, Huelga SC, et al. ALS-linked TDP-43 mutations produce aberrant RNA splicing and adult-onset motor neuron disease without aggregation or loss of nuclear TDP-43. *Proc Natl Acad Sci U S a*. 2013;110(8):E736-E745. doi:10.1073/pnas.1222809110
5. Neumann M, Sampathu DM, Kwong L, et al. Ubiquitinated TDP-43 in frontotemporal lobar degeneration and amyotrophic lateral sclerosis. *Science (80-)*. 2006;314(5796):130-133. doi:10.1126/science.1134108
6. Dadon-Nachum M, Melamed E, Offen D. The "dying-back" phenomenon of motor neurons in ALS. *J Mol Neurosci*. 2011;43(3):470-477. doi:10.1007/s12031-010-9467-1

13652990, 2023, 4, Downloaded from https://onlinelibrary.wiley.com/doi/10.1111/nan.12925 by Universidade Estadual Paulista, Wiley Online Library on [24/09/2026]. See the Terms and Conditions (https://onlinelibrary.wiley.com/terms-and-conditions) on Wiley Online Library for rules of use; OA articles are governed by the applicable Creative Commons License

7. Santosa KB, Keane AM, Jablonka-Shariff A, Vannucci B, Snyder-Warwick AK. Clinical relevance of terminal Schwann cells: an overlooked component of the neuromuscular junction. *J Neurosci Res*. 2018;96(7):1125-1135. doi:10.1002/jnr.24231
8. Bjornskov EK, Norris FH, Mower-Kuby J. Quantitative axon terminal and end-plate morphology in amyotrophic lateral sclerosis. *Arch Neurol*. 1984;41(5):527-530. doi:10.1001/archneur.1984.04050170073021
9. Tsujihata M, Hazama R, Yoshimura T, Satoh A, Mori M, Nagataki S. The motor end-plate fine structure and ultrastructural localization of acetylcholine receptors in amyotrophic lateral sclerosis. *Muscle Nerve*. 1984;7(3):243-249. doi:10.1002/mus.880070310
10. Yu H, Chen L, Zhang S, He J, Fan D. Early axonal dysfunction of the peripheral nervous system influences disease progression of ALS: evidence from clinical neuroelectrophysiology. *Front Neurol*. 2021;12(February):1, 574919-8. doi:10.3389/fneur.2021.574919
11. Jenkins TM, Alix JJP, Fingret J, et al. Longitudinal multi-modal muscle-based biomarker assessment in motor neuron disease. *J Neurol*. 2019;267(1):0123456789. doi:10.1007/s00415-019-09580-x
12. Philips T, Rothstein JD. Rodent models of amyotrophic lateral sclerosis. *Curr Protoc Pharmacol*. 2016;69. doi:10.1002/0471141755.ph0567s69.Rodent
13. Vinsant S, Mansfield C, Jimenez-Moreno R, et al. Characterization of early pathogenesis in the SOD1G93A mouse model of ALS: part II, results and discussion. *Brain Behav*. 2013;3(4):431-457. doi:10.1002/brb3.142
14. Narai H, Manabe Y, Nagai M, et al. Early detachment of neuromuscular junction proteins in ALS mice with SODG93A mutation. *Neurol Int*. 2009;1(1):16, e16. doi:10.4081/ni.2009.e16
15. Kanning KC, Kaplan A, Henderson CE. Motor neuron diversity in development and disease. *Annu Rev Neurosci*. 2010;33(1):409-440. doi:10.1146/annurev.neuro.051508.135722
16. Tosolini AP, Sleigh JN, Surana S, Rhymes ER, Cahalan SD, Schiavo G. BDNF-dependent modulation of axonal transport is selectively impaired in ALS. *Acta Neuropathol Commun*. 2022;10(1):121. doi:10.1186/s40478-022-01418-4
17. Alhindi A, Boehm I, Chaytow H. Small junction, big problems: neuromuscular junction pathology in mouse models of amyotrophic lateral sclerosis (ALS). *J Anat*. 2022;241(5):1089-1107. doi:10.1111/joa.13463
18. Arai T, Hasegawa M, Akiyama H, et al. TDP-43 is a component of ubiquitin-positive tau-negative inclusions in frontotemporal lobar degeneration and amyotrophic lateral sclerosis. *Biochem Biophys Res Commun*. 2006;351(3):602-611. doi:10.1016/j.bbrc.2006.10.093
19. Pamphlett R, Luquin N, McLean C, Jew SK, Adams L. TDP-43 neuropathology is similar in sporadic amyotrophic lateral sclerosis with or without TDP-43 mutations. *Neuropathol Appl Neurobiol*. 2009;35(2):222-225. doi:10.1111/j.1365-2990.2008.00982.x
20. Gordon D, Dafinca R, Scaber J, et al. Single-copy expression of an amyotrophic lateral sclerosis-linked TDP-43 mutation (M337V) in BAC transgenic mice leads to altered stress granule dynamics and progressive motor dysfunction. *Neurobiol Dis*. 2019;121(September 2018):148-162. doi:10.1016/j.nbd.2018.09.024
21. Ebstein SY, Yagudayeva I, Shneider NA. Mutant TDP-43 causes early-stage dose-dependent motor neuron degeneration in a TARDBP knockin mouse model of ALS. *Cell Rep*. 2019;26(2):364-373.e4. doi:10.1016/j.celrep.2018.12.045
22. Altman T, Ionescu A, Ibraheem A, et al. Axonal TDP-43 condensates drive neuromuscular junction disruption through inhibition of local synthesis of nuclear encoded mitochondrial proteins. *Nat Commun*. 2021;12(1):6914. doi:10.1038/s41467-021-27221-8
23. Wils H, Kleinberger G, Janssens J, et al. TDP-43 transgenic mice develop spastic paralysis and neuronal inclusions characteristic of ALS and frontotemporal lobar degeneration. *Proc Natl Acad Sci*. 2010;107(8):3858-3863. doi:10.1073/pnas.0912417107
24. Nijssen J, Comley LH, Hedlund E. Motor neuron vulnerability and resistance in amyotrophic lateral sclerosis. *Acta Neuropathol*. 2017;133(6):863-885. doi:10.1007/s00401-017-1708-8
25. Chaytow H, Carroll E, Gordon D, et al. Targeting phosphoglycerate kinase 1 with terazosin improves motor neuron phenotypes in multiple models of amyotrophic lateral sclerosis. *EBioMedicine*. 2022;83:104202. doi:10.1016/j.ebiom.2022.104202
26. Alhindi A, Boehm I, Forsythe RO, et al. Terminal Schwann cells at the human neuromuscular junction. *Brain Commun*. 2021;44(2):fcab081. doi:10.1093/braincomms/fcab081
27. Minty G, Hoppen A, Boehm I, et al. ANMJ-morph: a simple macro for rapid analysis of neuromuscular junction morphology. *R Soc Open Sci*. 2020;7(4):200128. doi:10.1098/rsos.200128
28. Jones RA, Reich CD, Dissanayake KN, et al. NMJ-morph reveals principal components of synaptic morphology influencing structure–function relationships at the neuromuscular junction. *Open Biol*. 2016;6(12):160240. doi:10.1098/rsob.160240
29. Feng G, Mellor RH, Bernstein M, et al. Neurotechnique imaging neuronal subsets in transgenic mice expressing multiple spectral variants of GFP variants with altered spectral properties and improved translational efficiency, thermostability, and quantum yield. As a result of these favorable pro. *Neuron*. 2000;28(1):41-51. doi:10.1016/S0896-6273(00)00084-2
30. Riessland M, Ackermann B, Förster AF, et al. SAHA ameliorates the SMA phenotype in two mouse models for spinal muscular atrophy. *Hum Mol Genet*. 2010;19(8):1492-1506. doi:10.1093/hmg/ddq023
31. Spiller KJ, Cheung CJ, Restrepo CR, et al. Selective motor neuron resistance and recovery in a new inducible mouse model of TDP-43 proteinopathy. *J Neurosci*. 2016;36(29):7707-7717. doi:10.1523/JNEUROSCI.1457-16.2016
32. Liu JX, Brännström T, Andersen PM, Pedrosa-Domellöf F. Distinct changes in synaptic protein composition at neuromuscular junctions of extraocular muscles versus limb muscles of ALS donors. *PLoS ONE*. 2013;8(2):e57473. doi:10.1371/journal.pone.0057473
33. Bruneteau G, Bauché S, Gonzalez de Aguilar JL, et al. Endplate denervation correlates with Nogo-A muscle expression in amyotrophic lateral sclerosis patients. *Ann Clin Transl Neurol*. 2015;2(4):362-372. doi:10.1002/acn3.179
34. Gould TW, Buss RR, Vinsant S, et al. Complete dissociation of motor neuron death from motor dysfunction by Bax deletion in a mouse model of ALS. *J Neurosci*. 2006;26(34):8774-8786. doi:10.1523/JNEUROSCI.2315-06.2006
35. Jones RA, Harrison C, Eaton SL, et al. Cellular and molecular anatomy of the human neuromuscular junction. *Cell Rep*. 2017;21(9):2348-2356. doi:10.1016/j.celrep.2017.11.008
36. Prasad A, Bharathi V, Sivalingam V, Girdhar A, Patel BK. Molecular mechanisms of TDP-43 misfolding and pathology in amyotrophic lateral sclerosis. *Front Mol Neurosci*. 2019;12(February):1-36. doi:10.3389/fnmol.2019.00025
37. Lattante S, Rouleau GA, Kabashi E. TARDBP and FUS mutations associated with amyotrophic lateral sclerosis: summary and update. *Hum Mutat*. 2013;34(6):812-826. doi:10.1002/humu.22319
38. Sreedharan J, Blair IP, Tripathi VB, et al. TDP-43 mutations in familial and sporadic amyotrophic lateral sclerosis. *Science (80-)*. 2008;319(5870):1668-1672. doi:10.1126/science.1154584
39. Van Deerlin VM, Leverenz JB, Bekris LM, et al. TARDBP mutations in amyotrophic lateral sclerosis with TDP-43 neuropathology: a genetic and histopathological analysis. *Lancet Neurol*. 2008;7(5):409-416. doi:10.1016/S1474-4422(08)70071-1
40. Huang C, Xia PY, Zhou H. Sustained expression of TDP-43 and FUS in motor neurons in rodent's lifetime. *Int J Biol Sci*. 2010;6(4):396-406. doi:10.7150/ijbs.6.396

13652990, 2023, 4, Downloaded from https://onlinelibrary.wiley.com/doi/10.1111/nan.12925 by Universidade Estadual Paulista, Wiley Online Library on [24/09/2026]. See the Terms and Conditions (https://onlinelibrary.wiley.com/terms-and-conditions) on Wiley Online Library for rules of use; OA articles are governed by the applicable Creative Commons License

41. Sephton CF, Good SK, Atkin S, et al. TDP-43 is a developmentally regulated protein essential for early embryonic development. *J Biol Chem*. 2010;285(9):6826-6834. doi:10.1074/jbc.M109.061846
42. Eréndira Avendaño-Vázquez S, Dhir A, Bembich S, Buratti E, Proudfoot N, Baralle FE. Autoregulation of TDP-43 mRNA levels involves interplay between transcription, splicing, and alternative polyA site selection. *Genes Dev*. 2012;26(15):1679-1684. doi:10.1101/gad.194829.112
43. Young AL, Vogel JW, Robinson JL, et al. Data-driven neuropathological staging and subtyping of TDP-43 proteinopathies. *Brain* Published online May 8. 2023;146(7):2975-2988. doi:10.1093/brain/awad145
44. Mackenzie IRA, Neumann M. Molecular neuropathology of frontotemporal dementia: insights into disease mechanisms from postmortem studies. *J Neurochem*. 2016;138:54-70. doi:10.1111/jnc.13588
45. Ling SC, Polymenidou M, Cleveland DW. Converging mechanisms in ALS and FTD: disrupted RNA and protein homeostasis. *Neuron*. 2013;79(3):416-438. doi:10.1016/j.neuron.2013.07.033
46. Fischer LR, Culver DG, Tennant P, et al. Amyotrophic lateral sclerosis is a distal axonopathy: evidence in mice and man. *Exp Neurol*. 2004;185(2):232-240. doi:10.1016/j.expneurol.2003.10.004
47. Masrori P, Van Damme P. Amyotrophic lateral sclerosis: a clinical review. *Eur J Neurol*. 2020;27(10):1918-1929. doi:10.1111/ene.14393
48. Pun S, Santos AF, Saxena S, Xu L, Caroni P. Selective vulnerability and pruning of phasic motoneuron axons in motoneuron disease alleviated by CNTF. *Nat Neurosci*. 2006;9(3):408-419. doi:10.1038/nn1653
49. Bolliger MF, Zurlinden A, Lüscher D, et al. Specific proteolytic cleavage of agrin regulates maturation of the neuromuscular junction. *J Cell Sci*. 2010;123(22):3944-3955. doi:10.1242/jcs.072090
50. Mech AM, Brown AL, Schiavo G, Sleigh JN. Morphological variability is greater at developing than mature mouse neuromuscular junctions. *J Anat*. 2020;237(4):603-617. doi:10.1111/joa.13228
51. Boehm I, Miller J, Wishart TM, et al. Neuromuscular junctions are stable in patients with cancer cachexia. *J Clin Invest*. 2020;130(3):1461-1465. doi:10.1172/JCI128411
52. Martin LJ, Wong M. Skeletal muscle-restricted expression of human SOD1 in transgenic mice causes a fatal ALS-like syndrome. *Front Neurol*. 2020;11(December):1, 592851-26. doi:10.3389/fneur.2020.592851
53. Kang H, Tian L, Mikesh M, Lichtman JW, Thompson WJ. Terminal Schwann cells participate in neuromuscular synapse remodeling during reinnervation following nerve injury. *J Neurosci*. 2014;34(18):6323-6333. doi:10.1523/JNEUROSCI.4673-13.2014

SUPPORTING INFORMATION

Additional supporting information can be found online in the Supporting Information section at the end of this article.

How to cite this article: Alhindi A, Shand M, Smith HL, et al. Neuromuscular junction denervation and terminal Schwann cell loss in the hTDP-43 overexpression mouse model of amyotrophic lateral sclerosis. *Neuropathol Appl Neurobiol*. 2023;49(4):e12925. doi:10.1111/nan.12925

13652990, 2023, 4, Downloaded from https://onlinelibrary.wiley.com/doi/10.1111/nan.12925 by Universidade Estadual Paulista, Wiley Online Library on [24/09/2026]. See the Terms and Conditions (https://onlinelibrary.wiley.com/terms-and-conditions) on Wiley Online Library for rules of use; OA articles are governed by the applicable Creative Commons License